

Short Note

Impulse Response of Civil Structures from Ambient Noise Analysis

by German A. Prieto, Jesse F. Lawrence, Angela I. Chung, and Monica D. Kohler

Abstract Increased monitoring of civil structures for response to earthquake motions is fundamental to reducing seismic risk. Seismic monitoring is difficult because typically only a few useful, intermediate to large earthquakes occur per decade near instrumented structures. Here, we demonstrate that the impulse response function (IRF) of a multistory building can be generated from ambient noise. Estimated shear-wave velocity, attenuation values, and resonance frequencies from the IRF agree with previous estimates for the instrumented University of California, Los Angeles, Factor building. The accuracy of the approach is demonstrated by predicting the Factor building's response to an M 4.2 earthquake. The methodology described here allows for rapid, noninvasive determination of structural parameters from the IRFs within days and could be used for state-of-health monitoring of civil structures (buildings, bridges, etc.) before and/or after major earthquakes.

Online Material: Movies of IRF and earthquake shaking.

Introduction

Determining a building's response to earthquake motions for risk assessment is a primary goal of seismologists and structural engineers alike (e.g., Cader, 1936a,b; Celebi *et al.*, 1993; Clinton *et al.*, 2006; Snieder and Safak, 2006; Chopra, 2007; Kohler *et al.*, 2007). Unfortunately, this method of risk assessment is limited by the amount of available data. A precious small number of instrumented buildings exist that have recorded actual earthquake motions (Dunand *et al.*, 2004), which can be used to verify building response. Wavefield-based seismic analysis of full-scale instrumented structures can yield important information for earthquake engineering: seismic velocity, frequency-dependent attenuation, resonant frequencies, and mode shapes (Snieder and Safak, 2006; Kohler *et al.*, 2007).

With increases in data quantity, computer power, and disk storage, seismologists recently began analyzing large volumes of ambient noise field data to determine the structure of the Sun (Rickett and Claerbout, 1999) and the Earth (e.g., Sabra *et al.*, 2005; Shapiro *et al.*, 2005; Yao *et al.*, 2006; Villaseñor *et al.*, 2007; Zheng *et al.*, 2008; Prieto *et al.*, 2009). Aki (1957) first proposed a method to study subsurface phase velocity beneath a seismic array using spatial autocorrelations. Later, Claerbout (1968) suggested that temporal averaging of these spatial correlations could yield impulse response functions (IRF). This technique requires analysis of large data volumes, which was computationally cumbersome until recently. Fundamentally, an IRF is an empirical function describing the propagation of waves through

an elastic medium from one point to another; traditionally, it is the response recorded at a receiver when a unit impulse is applied at a source location at time = 0.

In many studies using ambient vibrations from engineering structures (see Ivanovic *et al.*, 2000 and references therein), frequency domain analysis is performed to determine modal frequencies and mode shapes, sometimes including damping ratios. Usually, one would like to see if there are variations in modal parameters before and after major earthquakes (Snieder *et al.*, 2007) or before and after retrofitting (Celebi and Liu, 1998).

Traveling wave phase properties may also be useful for identifying damage by providing additional information about changes in elastic parameters that result in variations in wave speeds, travel times for specific phases (e.g., the initial direct shear wave), and reflection coefficients (e.g., Brenguier, Campillo, *et al.*, 2008). For example, Muto *et al.* (2007) showed numerically how the introduction of fractured welds on three floors of one wall of a finite-element model of a high rise subjected to small-amplitude earthquake excitation gave rise to a new propagating torsional wave. For elastic structures, traveling wave techniques to determine the location and time of occurrence of a high-frequency damage event that has been recorded on a seismic network (Kohler *et al.*, 2009; Heckman *et al.*, 2010) is not very common in the literature, as opposed to passive damage detection methods that do not rely on active sources (e.g., Sabra *et al.*, 2007; Nayeri *et al.*, 2008; Duroux *et al.*, 2010).

[Snieder and Safak \(2006\)](#) calculated IRFs by using interferometry on earthquake data from each floor in an instrumented building (the Millikan Library in Pasadena, California). Phase information allowed them to obtain the time domain IRF of the building and observe propagating waves inside it. More recently, [Michel et al. \(2008\)](#) compared building motions with predictions obtained through ambient vibrations. They used a frequency domain decomposition method for modal parameter analysis and were able to simulate the motion of the building due to a weak-to-moderate earthquake. Their study illustrates the limitations, however, of working solely in the spectral domain because of difficulties that often arise in trying to identify true spectral peak and spectral ratios, especially when the data are not broadband in nature.

Previous studies ([Snieder and Safak, 2006](#); [Kohler et al., 2007](#); [Snieder, 2009](#)) have obtained IRFs from recorded motions excited by an earthquake using interferometric methods. In this study, we demonstrate for the first time that IRFs for multistory buildings can also be retrieved using ambient noise only.

These IRFs can then be used to study (1) modal parameters of the building, (2) wave propagation inside the building, (3) estimates of the quality factor (Q) associated with the normal modes, and (4) predictions of building response to scenario ground motions of moderately sized earthquakes. Given the presence of continuous background noise generated by man-made and natural sources, only a short duration of time series data may be needed to obtain stable results.

This leads to the possibility of rapid structural monitoring through ambient vibrations without the need to wait for subsequent earthquakes as proposed in [Snieder et al. \(2007\)](#). As discussed by [Ivanovic et al. \(2000\)](#), monitoring using ambient vibrations has been used since the 1970s, mostly studying the modal shape variations. For example, [Nayeri et al. \(2008\)](#) determined modal parameters using ambient vibrations and observed a strong correlation of the parameter variations with temperature. Noise-correlation (interferometric) methods without active sources have also been tested in laboratory-scale mechanical systems. The impulse response of a metal hydrofoil due to changes in mounting conditions before and after large-amplitude load fluctuations was computed from high-frequency (> 400 Hz) ambient vibration cross correlations ([Sabra et al., 2007](#)).

Data Processing

The 17-story, steel, moment-frame Factor building at the University of California, Los Angeles, is instrumented with a 72-channel array of accelerometers in a unique structural state-of-health monitoring experiment ([Kohler et al., 2005, 2006](#)). The array records 100 samples-per-second data on a 24-bit digitizer for two pairs of north–south and east–west aligned accelerometers on most floors (with additional vertically aligned accelerometers on the bottom two floors).

Here, we analyze 50 complete days (between 1 October and 29 November 2004) of ambient noise data recorded on the

17 east–west channels along the southern wall of the Factor building. The sensor locations are shown in Figure 1. Factor array data have previously been analyzed for mode identification using ambient vibrations and earthquakes ([Kohler et al., 2005](#); [Skolnik et al., 2006](#); [Nayeri et al., 2008](#)). Twenty small-to-medium ($2.5 < M_L < 6.0$) earthquakes were recorded between 2004 and 2005, enabling calculation of impulse response functions with interferometric methods ([Kohler et al., 2007](#)). Different sources (such as wind and mechanical devices) also excite the building, enabling further estimation of dynamic characteristics ([Nayeri et al., 2008](#)). The Factor building array provides an excellent set of data with which we compare results from the new ambient noise technique with those of previous earthquake-based techniques.

Transfer Function and Impulse Response

The transfer function describing a linear medium's output response to an input force excitation provides an empirical impulse response function, $I(t)$, for the medium between the input, $f(t)$, and output, $u(t)$, locations ($u[t] = I[t] \times f[t]$) or $I[\omega] = u[\omega]/f[\omega]$ in the frequency response domain, e.g., [Meirovitch, 1997](#)). The IRF results from the constructive interference of signals from stationary source locations and destructive interference from nonstationary source locations. Time averaging over a longer duration for numerous random sources ensures a sufficiently uniform source distribution (e.g., [Campillo, 2006](#); [Bensen et al., 2007](#)).

[Snieder \(2009\)](#) discussed the advantages of analyzing the transfer function in the time domain rather than in the frequency domain. In Figure 2, for example, it is pretty clear that the waveforms represent the interference of upgoing and downgoing waves arriving from opposite arrival times. From the amplitude spectrum, this interpretation would not be trivial. Clearly, both domains provide complementary information about the impulse response of the building.

For each station and for each 10-min ambient noise data series, we compute impulse response functions with respect to the lowest floor along the south wall (sub-basement level). The results were averaged for 1-, 14-, 30-, and 50-day durations. In order to compensate for each source having varying amplitudes at each frequency, the 10-min subsets of the ambient noise field are normalized (i.e., whitened) per frequency using a multitaper technique ([Prieto et al., 2009](#)). To avoid the effects of transients, windows with large amplitudes are not used in calculating the IRF ([Prieto and Beroza, 2008](#)). Thus, the method presented here does not use large-amplitude shaking due to earthquakes but rather the ambient noise inside the building. Here, the transfer functions are averaged to generate IRFs for 1-, 14-, 30-, and 50-day durations.

Results

The ambient noise IRFs for the first 14 days of the data analyzed are shown in Figure 1 filtered for two frequency bands: 0.5–5.0 Hz and 1.0–3.0 Hz. The broader frequency

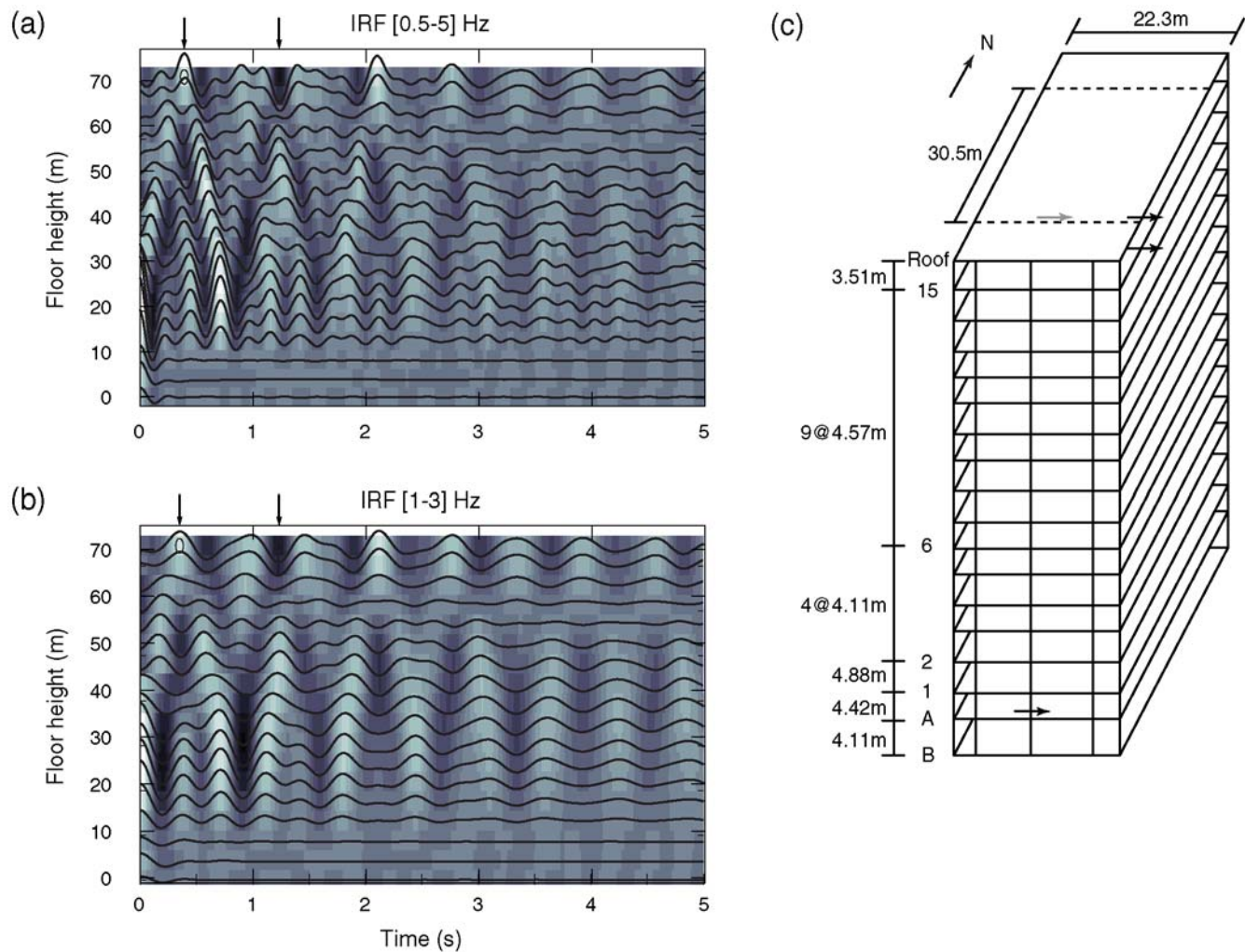


Figure 1. Impulse response functions calculated from 14 days of ambient noise plotted as positive and negative amplitudes for each floor over time. Panel (a) illustrates the IRFs for a broad frequency range (0.5–5 Hz), and panel (b) illustrates the resonance of the second harmonic (1.6 Hz). These IRFs are similar to those seen in figure 7b of Kohler *et al.* (2007). Arrows above each panel are used to estimate two-way travel times (upgoing waves) for the station at the roof with corresponding velocities of 177 and 169 m/s, respectively. Panel C) shows the locations of the east–west-component sensors. The gray arrow depicts the locations of the sensors for floors 1–14. The black arrows show the locations of the sensors on floors A, 15, and the roof. The color version of this figure is available only in the electronic edition.

range (0.5–5.0 Hz) represents the full range of predicted motions, whereas the narrower frequency range (1.0–3.0 Hz) accentuates the second east–west translational mode of the Factor building. Notably, the ambient noise IRFs are similar to those generated from earthquake interferometry (Kohler *et al.*, 2007), indicating that the method can provide comparable and independent results.

Shear-Wave Velocity

The measurable structural parameters also match those of interferometric methods (Kohler *et al.*, 2007). For example, the move-out of peak amplitudes for the IRFs illustrates a seismic shear-wave velocity of 180 m/s (Fig. 1). Here, we estimate the two-way travel time of seismic waves traveling from the top of the building down and up again (see picks in Fig. 1). We corroborate these results independently by

calculating the IRF with respect to the top floor (after Snieder and Safak, 2006) and use the peak amplitude of the downgoing waves (averaged for causal and acausal times) to estimate the wave speed (see Fig. 2). Similar results are obtained in both cases (177 m/s and 180 m/s, respectively, for the frequency range 0.5–5.0 Hz).

Resonant Frequencies and Attenuation

The resonance of the Factor building is also captured by the ambient noise IRFs. The average power spectrum for floors 4–13 (Fig. 3) shows peak amplitudes at 0.55, 1.6, 2.8, 4.2, and 5.2 Hz. The first three of these have been independently verified by a subspace state-space system identification method as the first three translational east–west resonant frequencies (Skolnik *et al.*, 2006).

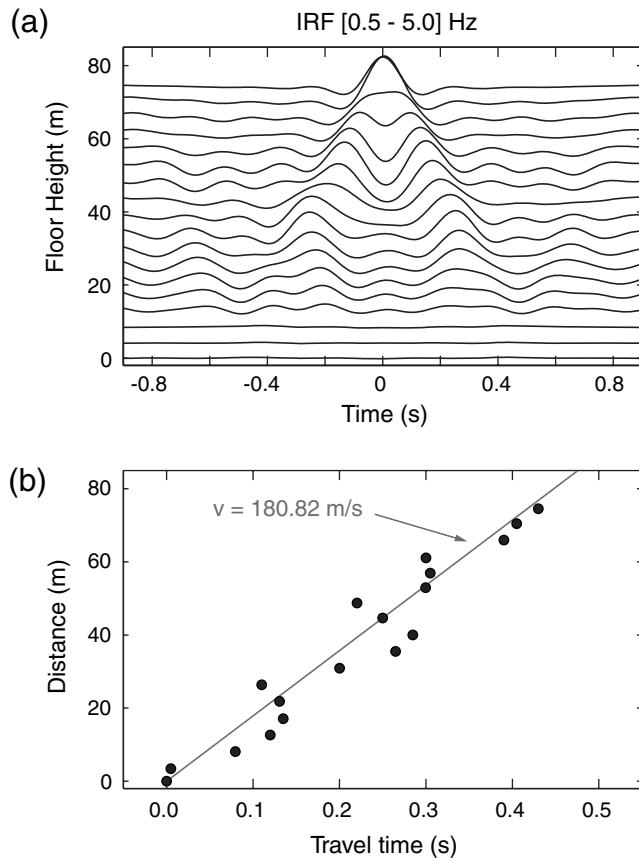


Figure 2. The seismic velocity estimation of the east–west component shear waves for the Factor building. Waveforms of the IRF with respect to the top floor (roof) are calculated, and the times of peak IRF amplitudes for the primary pulse are automatically picked for each floor from the 0.5–5 Hz filtered IRFs shown in (a). These times and the best-fit linear solutions to these time picks are shown in (b). The least-squares solution to the slope is $180 \pm 10 \text{ ms}^{-1}$, representing the standard deviation.

For each resonant frequency, the quality factor is calculated from the amplitude decay with time and seismic velocity. The IRFs are filtered around the resonant frequencies, and the envelope is plotted (Fig. 3b). The amplitude decay with time (slope in Fig. 3b) is related to the attenuation as $Q = \omega / (2 \times \text{slope})$, where $\omega = 2\pi f$ and f are the resonant frequencies. By using different floors, we may obtain uncertainty measurements. The consistency of Q values for each floor (Fig. 3c) illustrates the accuracy of the measurement.

A histogram of the estimated quality factors (Fig. 3b) illustrates an average Q of 25.0 and a small uncertainty (± 0.3) for the second mode. The Q for the first and third modes is 37.8 ± 5.0 and 34.1 ± 15.3 , respectively. The attenuation value for the second mode ($Q = 25 \pm 0.3$) is larger than those of Kohler *et al.* (2007) who obtained $Q \sim 16$, corresponding to a damping ratio of 3%. The discrepancy is most likely due to frequency-dependent variations between the earthquake and ambient vibration data, as well as numerical instabilities in the earthquake-derived amplitude curves. It is within the range of damping ratios for the first six translational modes (1.3%–8.3% corresponding to a frequency

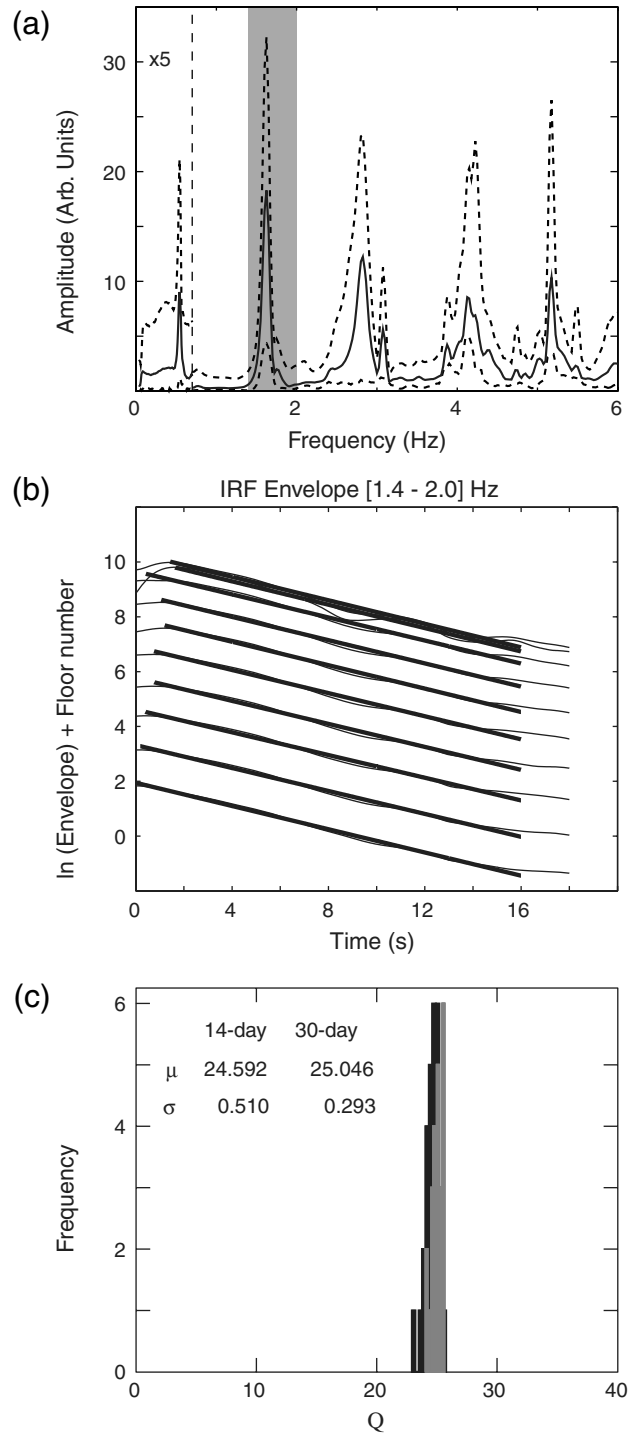


Figure 3. The east–west translational mode frequencies of the building are clearly visible in (a) the average (continuous line), maximum, and minimum (dashed) amplitude spectra. Spectral peaks are clearly observed around 0.55, 1.6, 2.8, 4.2, and 5.2 Hz. The peak amplitudes of the normal modes vary per floor according to proximity to the nodal points. The amplitude spectrum below 0.7 Hz (dashed vertical line) is multiplied by 5. The attenuation of the second mode is measured in (b) as the time rate of change of the envelope of the filtered records for floors 4–13. The measured slope for each floor yields a (c) quality factor of 25.0 ± 0.3 ($Q = -\omega/2$ slope) for a 30-day time period and 24.6 ± 0.5 for the 14-day time period.

range of 0.54–3.1 Hz) obtained by system identification from ambient vibration records (Skolnik *et al.*, 2006).

Building's Response Prediction

There are multiple reflected phases within the building, including a particularly strong reflection at the top, bottom, and tenth floor (see Fig. 1). The reflections off the bottom floor are reverse polarity so that the primary signal (bottom to top and back again) alternates from positive to negative. These observations agree with those by Kohler *et al.* (2007) and can be straightforwardly explained by a reflection off the building's fixed-base foundation boundary. There is no evidence of significant soil–structure interactions in response to the low-amplitude excitations recorded to date.

To test the ability of the IRFs to predict earthquake motions for a given scenario, we compare records from an observed earthquake (13 November 2004 M_L 4.2) to the convolution of the basement-level record with the previously obtained IRFs for each floor (Fig. 4). The low root-mean-square (rms) misfit (23%) between predicted and observed records indicates that the ambient noise IRFs can accurately forecast a building's response to a moderate earthquake (Michel *et al.*, 2008). Whereas the IRFs are useful when illustrated as static images, such as Figures 1 or 4, the true dynamic response of the Factor building is better described in  movies of predicted motion available in the electronic supplement to this paper. From such movies, it is clear that some floors are particularly sensitive to earthquake vibration at particular frequencies, whereas others are not, in agreement with (Kohler *et al.*, 2007).

IRF Stability

We have found that the results are independent of day selection, provided that sufficient data quantities are used. Figure 5 illustrates the IRF improvement with data quantity in which misfit reduction is typically >90% after 14 days with respect to the 50-day IRF. The duration required to generate stable IRFs can be significantly shorter (days to weeks) than the unpredictable duration between local earthquakes (months to years, depending on location). Additionally, acceleration records longer than 14 days provide independent data for uncertainty analysis. Note that the rate of IRF convergence may vary for different structures due to dissimilar design, usage, and environment.

Discussion and Conclusions

The immediate availability of useful data for application of the ambient noise method in structural analysis offers several unique benefits to society. Primarily, the shorter wait for enough time series data required by the method will allow more buildings to be analyzed with campaign-style, rapidly deployable, temporary arrays rather than (semi) permanent arrays (Ivanovic and Trifunac, 1995). The main difference between the method proposed here and other interferometry

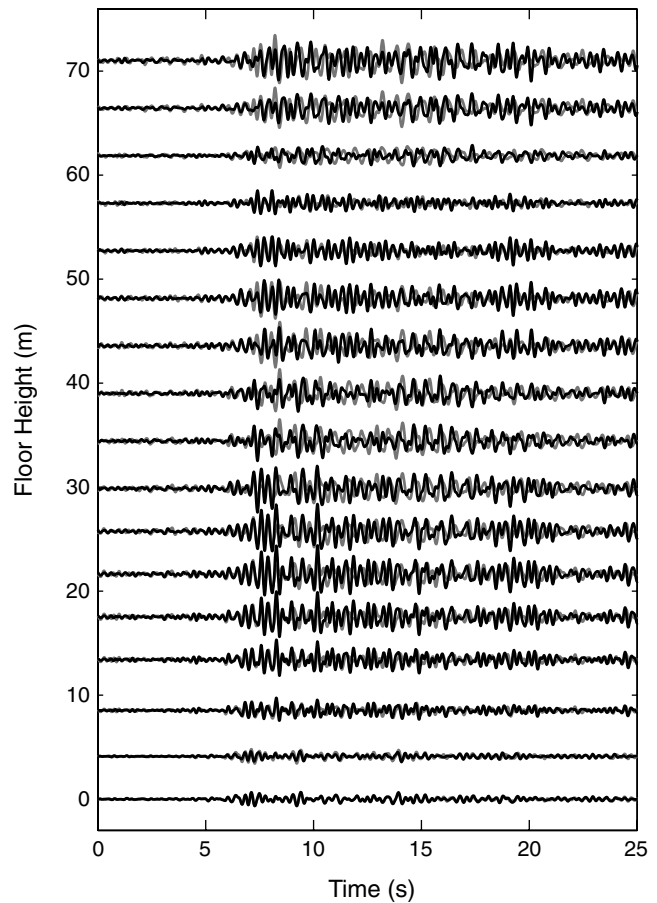


Figure 4. Predicted building displacements for each floor calculated by convolving the impulse response functions with the 14 November 2004 M 4.2 earthquake record from the lowermost floor. Predicted displacements (black) are highly similar (23% rms misfit) to the observed displacements (gray) for that earthquake. Note that predicted motions for floors 1–15 are phase delayed by 0.04 s, which corresponds to the time delay for a source defined at the basement level rather than the sub-basement level.

studies in buildings (Snieder and Safak, 2006; Kohler *et al.*, 2007; Snieder *et al.*, 2007) is that the data in previous studies use earthquake shaking, whereas we exclusively use ambient vibrations. Consequently, this method can also be used to perform propagating-wave-based system identification of buildings to complement modal-based methods, which is of key importance for damage assessment (Skolnik *et al.*, 2006). With the rapidly decreasing price and installation time of both microelectromechanical systems accelerometers and data acquisition technology (e.g., Paek *et al.*, 2006; Cochran *et al.*, 2009), campaign-style, ambient noise building monitoring may soon become a new seismic risk industry. Alternatively, within the time it might take to record an earthquake (months to years), a reconfigurable array of sensors could yield dozens to hundreds more ambient noise IRFs for the same structure, providing greater resolution of structural parameters.

Predictions of structural motion calculated from the structure's ambient vibration IRFs convolved with hypothetical or previously observed weak-to-moderate ground-motion time

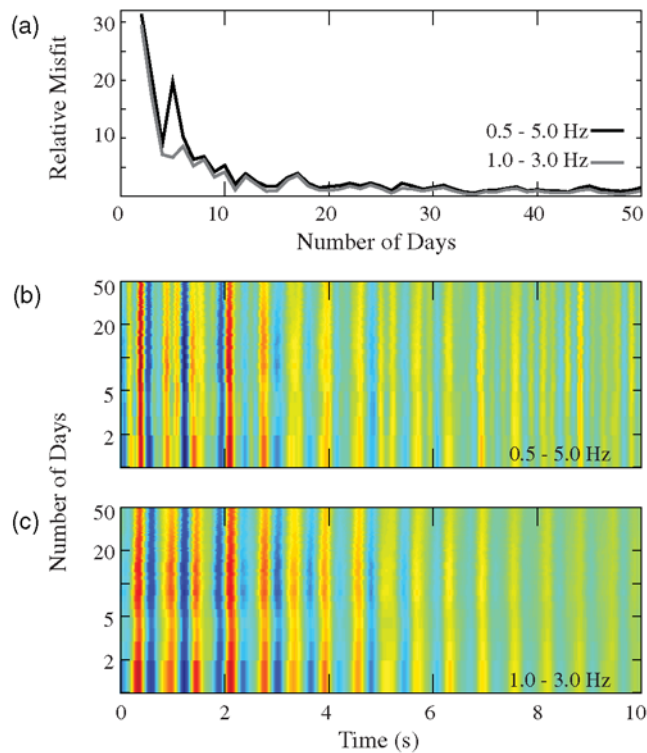


Figure 5. Convergence of IRF as a function of length of data. (a) Relative misfit of IRF with respect to the 50-day stack IRF; (b) and (c) are the cumulative IRFs between the basement and roof receivers at frequency bands 0.5–5 Hz and 1–3 Hz, respectively. IRF convergence is proportional to the square root of the subset data quantity. This is true for a broad range of frequencies. The color version of this figure is available only in the electronic edition.

histories could lead to predictions of the onset of inelastic behavior through, for example, the computation of interstory drift (Michel *et al.*, 2008). With a single permanent accelerometer on the basement floor, the predicted building motions may be estimated after the next occurrence of a potentially damaging earthquake in the future. The convolution of theoretical ground motion from any given rupture scenario (earthquake-to-floorboard; e.g., Jones *et al.*, 2008) with the structural IRFs (floorboard-to-rafter) would predict possible scenarios from earthquake-to-rafter. Similarly, the convolution of subsurface ambient noise IRFs (Prieto and Beroza, 2008) and the structural IRFs could also yield empirical earthquake-to-rafter IRFs when a secondary sensor (a virtual source; e.g., Prieto and Beroza, 2008) is placed near an active fault.

The IRFs calculated from ambient noise or small-to-moderate earthquake interferometry (Snieder and Safak, 2006; Kohler *et al.*, 2007) only evaluate the behavior of structural parameters in the linear response regime. Once interstory drift increases well beyond the linear regime, the structural parameters rapidly become nonlinear (Shome *et al.*, 1998). After such a large-amplitude event, changes to measurable parameters such as seismic velocity (Brennguier, Campillo, *et al.*, 2008; Brennguier, Shapiro, *et al.*, 2008), resonant fre-

quencies (Clinton *et al.*, 2006), and attenuation could be evaluated with a second campaign-style experiment. State-of-health monitoring could observe such changes immediately following or well after a major earthquake but would not require aftershock data.

In summary, ambient noise analysis with campaign-style data could lead to denser observations of structural parameters. Because the ambient noise IRF method does not require permanent or invasive sensors, many more structures could be studied in greater detail, resulting in an improved understanding of structural response and earthquake risk.

Data and Resources

Seismograms used in this study are made available thanks to operations and maintenance supported by personnel and funds from the U.S. Geological Survey Advanced National Seismic System (Grant 05HQGR0159) program and the National Science Foundation (NSF) Center for Embedded Networked Sensing at the University of California, Los Angeles (UCLA). Data can be obtained the Incorporated Research Institutions for Seismology (IRIS) Data Management Center at www.iris.edu (last accessed January 2008).

Acknowledgments

The authors would like to thank two anonymous reviewers and the editor for thorough reviews that improved the paper.

References

- Aki, K. (1957). Space and time spectra of stationary stochastic waves with special reference to microtremors, *Bull. Earthq. Res. Inst.* **35**, 415–457.
- Bensen, G. D., M. H. Ritzwoller, M. P. Barmin, A. L. Levshin, F. Lin, M. P. Moschetti, N. M. Shapiro, and Y. Yang (2007). Processing seismic ambient noise data to obtain reliable broad-band surface wave dispersion measurements, *Geophys. J.* **169**, 1239–1260, doi [10.1111/j.1365-246X.2007.03374.x](https://doi.org/10.1111/j.1365-246X.2007.03374.x).
- Brennguier, F., M. Campillo, C. Hadziioannou, N. M. Shapiro, R. M. Nadeau, and E. Larose (2008). Postseismic relaxation along the San Andreas fault at Parkfield from continuous seismological observations, *Science* **321**, 1478–1481.
- Brennguier, F., N. M. Shapiro, M. Campillo, V. Ferrazzini, Z. Duputel, O. Coutant, and A. Nercessian (2008). Towards forecasting volcanic eruptions using seismic noise, *Nature Geosciences* **1**, doi [10.1038/ngeo104](https://doi.org/10.1038/ngeo104), 126–130.
- Cader, D. S. (1936a). Observed vibration of buildings, *Bull. Seismol. Soc. Am.* **26**, no. 4, 245–267.
- Cader, D. S. (1936b). Observed vibration of bridges, *Bull. Seismol. Soc. Am.* **26**, no. 4, 267–289.
- Campillo, M. (2006). Phase and correlation in random seismic fields and the reconstruction of the Green Function, *Pure Appl. Geophys* **163**, 475–502, doi [10.1007/s00024-005-0032-8](https://doi.org/10.1007/s00024-005-0032-8).
- Çelebi, M., and H. P. Liu (1998). Before and after retrofit response of a building during ambient and strong motions, *J. Wind Eng. Ind. Aerodyn.* **77–78**, 259–268.
- Çelebi, M., L. T. Phan, and R. D. Marshall (1993). Dynamic characteristics of five tall buildings during strong and low-amplitude motions, *Struct. Des. Tall Build.* **2**, 1–15, doi [10.1002/tal.4320020102](https://doi.org/10.1002/tal.4320020102).
- Chopra, A. K. (2007). *Dynamics of structures: Theory and Applications to Earthquake Engineering*, Third Ed., Prentice-Hall, New Jersey.

- Claerbout, J. F. (1968). Synthesis of a layered medium from its acoustic transmission response, *Geophysics* **33**, no. 2, 264–269.
- Clinton, J. F., S. C. Bradford, T. H. Heaton, and J. Favela (2006). The observed wander of the natural frequencies in a structure, *Bull. Seismol. Soc. Am.* **96**, 237–257.
- Cochran, E. S., J. F. Lawrence, C. Christensen, and R. S. Jukka (2009). The Quake-Catcher Network: Citizen science expanding seismic horizons, *Seismol. Res. Lett.* **80**, 26–30.
- Dunand, F., J. E. Rodgers, A. V. Acosta, M. Salsman, P.-Y. Bard, and M. Celebi (2004). Ambient vibration and earthquake strong-motion data sets for selected USGS Extensively instrumented buildings, *U.S. Geol. Surv. Open-File Rept. 2004-1375*.
- Duroux, A., K. G. Sabra, J. Ayers, and M. Ruzzene (2010). Extracting guided waves from cross-correlations of elastic diffuse fields: Applications to remote structural health monitoring, *J. Acoust. Soc. Am.* **122**, 204–215.
- Heckman, V. M., M. D. Kohler, and T. H. Heaton (2010). Detecting failure events in buildings: A numerical and experimental analysis, *9th and 10th U.S. National and 10th Canadian Conference on Earthquake Engineering*, Toronto, 25–29 July 2010.
- Ivanovic, S. S., and M. D. Trifunac (1995). Ambient vibration surveys of full-scale structures using personal computers—Examples for Kaprielian Hall, *Report Number CE 95-05 USC*, Los Angeles, California, 108 pp.
- Ivanovic, S. S., M. D. Trifunac, and M. I. Todorovska (2000). Ambient vibration tests of structures—A review, *ISSET J. Earthq. Tech.* **37**, no. 4, 165–197.
- Jones, L. M., R. Bernknopf, D. Cox, J. Goltz, K. Hudnut, D. Mileti, S. Perry, D. Ponti, K. Porter, M. Reichle, H. Seligson, K. Shoaf, J. Treiman, and A. Wein (2008). The Shakeout scenario, in *U.S. Geol. Surv. Open-File Rept. 2008-1150 and California Geol. Surv. Preliminary Report 25*, <http://pubs.usgs.gov/of/2008/1150/>.
- Kohler, M. D., P. M. Davis, and E. Safak (2005). Earthquake and ambient vibration monitoring of the steel frame UCLA Factor building, *Earthq. Spectra* **21**, 715–736.
- Kohler, M. D., T. H. Heaton, and S. C. Bradford (2007). Propagating waves in the steel, moment-frame Factor building recorded during earthquakes, *Bull. Seismol. Soc. Am.* **97**, 1334–1345.
- Kohler, M., T. Heaton, R. Govindan, P. Davis, and D. Estrin (2006). Using embedded wired and wireless seismic networks in the moment-resisting steel frame Factor building for damage identification, in *Proc. of the 4th China-Japan-U.S. Symposium on Structural Control and Monitoring*, 16–17 October 2006.
- Kohler, M. D., T. H. Heaton, and V. Heckman (2009). A time-reversed reciprocal method for detecting high-frequency events in civil structures with accelerometer arrays, *Proc. of the 5th International Workshop on Advanced Smart Materials and Smart Structures Technology*, Boston, Massachusetts, 30–31 July 2009.
- Meirovitch, L. (1997). *Principles and Techniques of Vibrations*, Prentice Hall, New York.
- Michel, C., P. Guéguen, and P.-Y. Bard (2008). Dynamic parameters of structures from ambient vibration measurements: An aid for the seismic vulnerability assessment of existing buildings in moderate seismic hazard regions, *Soil Dyn. Earthq. Eng.* **28**, 593–604.
- Muto, M., T. Heaton, S. Krishnan, and M. Kohler (2007). Structural damage detection using numerical techniques: Prototype study of the UCLA Factor building (poster presentation), *SCEC Annual Meeting*, Palm Springs, California, 8–12 September 2007.
- Nayeri, R. D., S. F. Masri, R. G. Ghanem, and R. L. Nigbor (2008). A novel approach for the structural identification and monitoring of a full-scale 17-story building based on ambient vibration measurements, *Smart Mater. Struct.* **17**, 19 p.
- Paek, J., O. Gnawali, K.-Y. Jang, D. Nishimura, R. Govindan, J. Caffrey, M. Wahbeh, and S. Masri (2006). A programmable wireless sensing system for structural monitoring, in *4th World Conference on Structural Control and Monitoring (4WCSCM)*, San Diego, California.
- Prieto, G. A., and G. C. Beroza (2008). Earthquake ground motion prediction using the ambient seismic field, *Geophys. Res. Lett.* **35**, L14304, doi [10.1029/2008GL034428](https://doi.org/10.1029/2008GL034428).
- Prieto, G. A., J. F. Lawrence, and G. C. Beroza (2009). Anelastic earth structure from the coherency of the ambient seismic field, *J. Geophys. Res.* **114**, B07303, doi [10.1029/2008JB006067](https://doi.org/10.1029/2008JB006067).
- Prieto, G. A., R. L. Parker, and F. L. Vernon (2009). A Fortran 90 library for multitaper spectrum analysis, *Comput. Geosci.* **35**, 1701–1710.
- Rickett, J., and J. Claerbout (1999). Acoustic daylight imaging via spectral factorization; Helioseismology and reservoir monitoring, *TLE* **18**, no. 8, 957–960.
- Sabra, K. G., E. S. Winkel, D. A. Bourgoyne, B. R. Elbing, S. L. Ceccio, M. Perlin, and D. R. Dowling (2007). Using cross correlations of turbulent flow induced vibrations or structural health monitoring, *J. Acoust. Soc. Am.* **121**, 1987–1995, doi [10.1121/1.2710463](https://doi.org/10.1121/1.2710463).
- Sabra, K. G., P. Gerstoft, P. Roux, W. A. Kuperman, and M. C. Fehler (2005). Surface wave tomography from microseisms in southern California, *Geophys. Res. Lett.* **32**, L14,311, doi [10.1029/2005GL023155](https://doi.org/10.1029/2005GL023155).
- Shapiro, N., M. Campillo, L. Stehly, and M. Ritzwoller (2005). High-resolution surface wave tomography from ambient seismic noise, *Science* **307**, 1615–1618.
- Shome, N., C. A. Cornell, P. Bazzurro, and J. E. Carballo (1998). Earthquakes, records, and nonlinear responses, *Earthq. Spectra* **14**, no. 3, 469–500.
- Skolnik, D., Y. Lei, E. Yu, and J. W. Wallace (2006). Identification, model updating, and response prediction of an instrumented 15-story steel-frame building, *Earthq. Spectra* **22**, no. 3, 781–802.
- Snieder, R. (2009). Extracting the time-domain building response from random vibrations, in *Coupled Site and Soil-Structure Interaction Effects with Application to Seismic Risk Mitigation*, T. Schanz and R. Iankov (Editors), SpringerNew York, 283–292.
- Snieder, R., and E. Safak (2006). Extracting the building response using seismic interferometry: Theory and application to the Millikan library in Pasadena, California, *Bull. Seismol. Soc. Am.* **96**, 586–598.
- Snieder, R., S. Hubbard, M. Haney, G. Bawden, P. Hatchell, and A. RevilDOE Geophysical Monitoring Working Group (2007). Advanced non-invasive geophysical monitoring techniques, *Ann. Rev. of Earth Planet. Sci.* **35**, 653–683.
- Villaseñor, A., Y. Yang, and M. H. Ritzwoller (2007). Ambient noise surface wave tomography of the Iberian Peninsula: Implications for shallow seismic structure, *Geophys. Res. Lett.* **34**, L11,304, doi [10.1029/2007GL03016](https://doi.org/10.1029/2007GL03016).
- Yao, H., R. D. van der Hilst, and M. V. de Hoop (2006). Surface-wave array tomography in SE Tibet from ambient seismic noise and two-station analysis I. Phase velocity maps, *Geophys. J. Int.* **166**, 732–744.
- Zheng, S., X. Sun, X. Song, Y. Yang, and M. H. Ritzwoller (2008). Surface wave tomography of china from ambient seismic noise correlation, *Geochem. Geophys. Geosyst.* **9**, Q05,020, doi [10.1029/2008GC001981](https://doi.org/10.1029/2008GC001981).

Departamento de Física
 Universidad de los Andes
 Calle 18A 1–10, Of. Ip301
 AA 4976, Bogotá, Colombia
 (G.A.P.)

Department of Geophysics
 Stanford University
 397 Panama Mall
 Stanford, California 94306
 (J.F.L., A.I.C.)

Center for Embedded Networked Sensing
 University of California at Los Angeles
 Los Angeles, California 90095-1596
 (M.D.K.)